

Fouling Simulations of a Passive Part of the Testing Combustion Facility

Jiří Strouhal*, Tomáš Juřena, Zdeněk Jegla

Brno University of Technology, Institute of Process Engineering, Technická 2, 61669 Brno, Czech Republic

* strouhal@fme.vutbr.cz

Results from the previous work of Strouhal et al. (2020) suggest that the used CFD fouling model together with user-implemented subroutines is not sufficient for obtaining satisfactory agreement with deposits observed in a described experimental device. The objective of this work is to create a basis for qualitative improvements of the simulation results. This includes using more detailed geometry and testing an influence of variation of parameters of two implemented fouling models. An accurate estimation of these parameters requires either empirical evidence from device operation or detailed information about fly ash composition and properties, which is usually accessible only for individual fly ash constituents. The goal of the sensitivity analysis was to show influence of these parameters on deposition rates, identify insignificant parameters for the tested range of particle properties and diameters and the most significant parameters for each of the six tested fly ash size fractions. To the authors' knowledge, such an analysis is not present in available literature. The first tested model shown that one parameter to be significantly higher compared to other, except for the smallest particles. For the second model, all parameters were found to be significant at least for one examined particle diameter. Elastic deformation, plastic deformation and adhesion are thus considered important across the tested range of particle properties and sizes, at least for the fouling model used.

1. Introduction

Usage of alternative solid fuels provides savings in primary fuels due to using renewable sources. Variability in composition and amounts of waste combustion products causes difficult predictability of instant release of these products, which causes difficulties in usage of these fuels (Stančín et al., 2020). Fouling has to be considered when designing devices such as heat exchangers used in industrial boilers. It influences size and total cost of the facility (Stehlík, 2011). CFD in fouling prediction was used by many authors. A list of various examples of fouling models based on CFD can be found in an extensive review done by Cai et al. (2018). Models of particulate matter fouling can differ among other by purpose of their usage. The most advanced models are useful for (possibly dynamic) simulation of deposit growth and its influence on the flow field, heat transfer and pressure loss. Often it is desirable to determine conditions, for which particle deposition can be significantly reduced by adjusting the heat transfer surface design or operating conditions (Jegla et al., 2010).

Fouling in an experimental device installed on the Institute of Process Engineering is modelled. This device consists of three main parts: a rotary kiln, deposition chamber and a heat exchanger. The chamber represents a passive mechanical part for retaining of the PM. Modelling focused on the chamber and rear part of the kiln. The present study extends the authors' previous work on development of a CFD model for the prediction of fouling in heat exchangers by particulate matter (PM). This model should be applicable to typical fouling problems on the flue gas side on industrial scale. Hence, cost-effective models were adopted from literature. Preliminary simulation results were not satisfactory compared to experimental findings, which was most obvious for the bottom of a part of an experimental device. The predicted deposition flow rate was very low compared to other surfaces, while experiment has shown this surface to be the most fouled part of the chamber. The objective of this work is to investigate sensitivity of the predicted deposition mass flow rate on variation of parameters of two fouling models. To best authors' knowledge, such an analysis is not present in available literature. Reference values were chosen with respect to typical fly ash components and conditions inside convective sections of industrial boilers.

2. Model

All simulations were conducted on a single model of the kiln and chamber assembly. The initial stage of fouling was considered, for which the internal geometry is not affected by accumulated matter. Two models are described, each using small number of parameters describing properties of particles and wall surface.

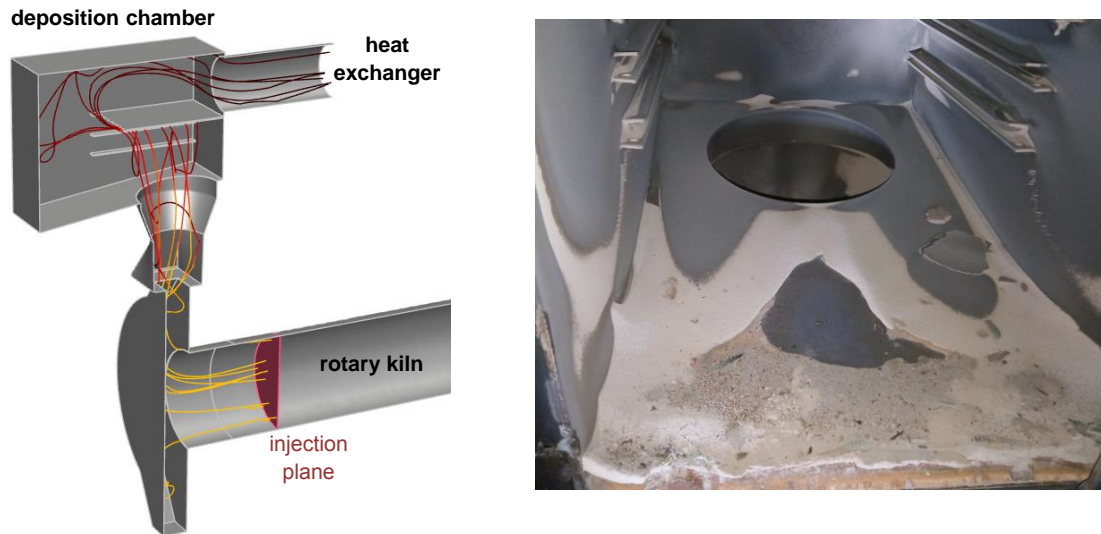


Figure 1: Geometry of the kiln outlet and deposition chamber with illustrative particle trajectories and location of particle injection plane, used in CFD simulations (left); observed deposit after combustion tests in 2020, showing approximately symmetric pattern (right).

In order to reduce the time required for simulations, only half of the geometry was modelled, assuming planar symmetry of the investigated flow and particle trajectory patterns. This assumption is partially supported by the symmetry of deposits formed in the chamber during the combustion tests. The generated mesh consisted of $2 \cdot 10^6$ cells. For near wall regions, 6 to 12 prismatic layers were used, with uniform height of boundary cells' layer. Polyhedral cells were used for the rest of the domain. The smallest boundary cell height was set to 0.15 mm, which presents a value larger than the radius of the largest injected particle, preventing an unrealistic "submersion" of the particle under the wall surface. The average value of y^+ at boundary cell centroids was 0.59 for the whole domain and 0.56 for the chamber, with 0.05 % of cells with $y^+ \geq 4$ in the whole domain and zero in the chamber. The whole fouling model was implemented in Ansys® Fluent 2020 R2 (Ansys, 2020), combined with User Defined Functions, including C routines for modelling of the particle deposition.

2.1 Flow model and DPM

For modelling of the turbulence, the Realizable k - ϵ model combined with an Enhanced Wall Treatment was used. Note, that although the use of the RANS models in general leads to shorter computational time, it often overpredicts the deposition flow rates (Weber et al., 2013). For simulations of PM transport, the steady Discrete Phase Model (DPM) was used. Influence of the turbulence on the particle motion was simulated by using Discrete Random Walk Model (DRWM) combined with Random Eddy Lifetime model using Time Scale Constant 0.15. The number of tries was set to 25, providing a compromise between detailed picture of deposition mass flux and the required computational time. The total number of injected particles. Investigation of the exact location of PM source was not among objectives of this work. Particles were injected from a plane located 0.4 m from the kiln hopper, as shown on Figure 1.

2.2 Model WK12

This fouling model can be found in the work of Waclawiak and Kalisz (2012). It was originally designed for simulations of fouling of superheater tubes in a convective part of industrial boiler. The criterion for particle deposition is based on a force balance, derived from energy balance. Particle sticks if a sum of normal components (relative to the wall or deposit surface) of a gravitational force $F_{g,n} = m_p g \cos \alpha$ and Van der Waals force $F_{VW} = 2 B / (3 d_p)$ acting on a particle exceeds so-called elastic rebound force, expressed by Eq(1). The g is gravitational acceleration, θ is the impact angle, d_p is the particle diameter and B is an empirical constant. Particle sticking probability is expressed by Eq(2). Only B , n and d_{ref} were selected for factorial analysis.

The effect of change of a constant G can be substituted by variation of d_{ref} , requiring eight instead of 16 simulations.

$$F_{el} = G (d_p/d_{ref})^n d_p^2 |v_{i,n}|^{1.2} \quad (1)$$

$$p = \begin{cases} 1, & F_{vw} + F_{g,n} \geq F_{el} \\ 0, & \end{cases} \quad (2)$$

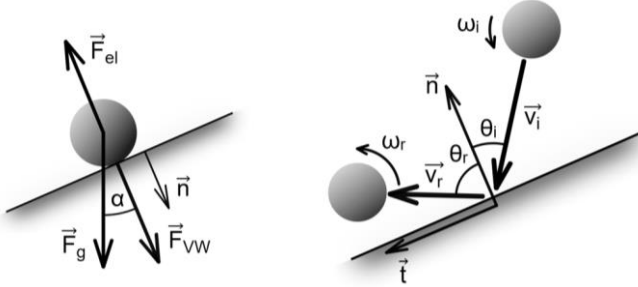


Figure 2: Forces considered in the WK12 model (left) and kinematics in the TN98X18 model (right).

2.3 Model TN98X18

The model described by authors Thornton and Ning (1998) was derived for normal impacts of adhesive particles on a smooth surface, assuming elastic deformations of the impacted surface and elastic or perfectly plastic deformation of the particle. In this work, their model was used for calculation of the rebound velocity normal component. Adhesion occurs during the contact, causing energy losses, further increased if the plastic deformation occurs. Model further assumes the particle geometry changes only negligibly. The expression for the normal restitution coefficient differs between three impaction regimes, determined by velocity values. The first is the sticking velocity v_s , which is the minimum velocity, for which the particle rebounds. The second is the yield velocity v_y , over which a plastic deformation occurs. These velocities can be obtained from particle and surface properties (Eq(3) and Eq(4)).

$$v_s = 1.84 \left((\Gamma/r_p)^5 / (\rho_p^3 E^{*2}) \right)^{1/6} \quad (3)$$

$$v_y = 1.56 (p_y^5 / (\rho_p E^{*4}))^{0.5} \quad (4)$$

Unlike the WK12 model, which was designed and tested even for oblique impacts by Waclawiak and Kalisz (2012), the original model of Thornton and Ning (1998) was originally proposed and tested for normal impacts and so, it was adjusted by adding sub-model for calculation of a tangential component of the rebound velocity, described by Xie et al. (2018), also accounting for the particle rotation. Assumptions of the sub-model include spherical shape of particles, particle rotation axis normal to impact and rebound velocity vectors, Coulombic friction during the impact and the independency of the normal restitution coefficient on the impact angle. Expressions for the ratio of the dynamic friction coefficient and impulse ratio required for the momentum balance of the particle during impact were determined for ash particles and smooth steel surface. Experiments were conducted for fly-ash diameters in range (47 to 53) μm , impact velocities (2.2, 3.4 and 4.22) m/s and impact angles in range (15 to 75) $^\circ$.

3. Model setup and results

The average value of the measured flue gas mass flow rate was 0.120 kg s^{-1} . The gas density and temperature were 0.343 kg m^{-3} and $752 \text{ }^\circ\text{C}$, estimated from the average of series of measurements at the kiln outlet. The gas dynamic viscosity $4.227 \cdot 10^{-5} \text{ Pa s}$ was estimated from the temperature assuming similar temperature dependency as air. A uniform mass flux was defined at the kiln inlet, with turbulence intensity and hydraulic diameter set to 5 % and 0.4 m, respectively. With respect to absence of heat transfer surfaces in investigated parts of the experimental device and neglecting the combustion process in the kiln, the flow was modelled as isothermal.

As in the previous work of Strouhal et al. (2020), the ash properties were taken from work of Raclavská et al. (2017), describing fly ash from the municipal solid waste combustion, providing a particle size distribution, composition and density. Six size fractions were assumed, each with uniform size distribution, with diameter

equal to arithmetic mean of every interval reported by Raclavská et al. (2017), yielding six particle diameters: 6, 14, 19.5, 28.5, 41.5 and 74.5 μm .

For each fouling model, nine simulations were conducted. The observed quantity was the total deposition mass flow rate in the rear part of kiln and the deposition chamber. Both series of simulations present sensitivity analysis of the model with respect to variation of selected model parameters. The analysis required one simulation with parameters set to reference values, followed by eight simulations for all combinations of maxima and minima of these parameters, representing their variation of 50 % of reference values.

Table 1: Mean values of model parameters with references to literature

Model	Parameter	Value	Reference	Note
WK12	B	10^{-17}	(Waclawiak and Kalisz 2012)	-
	n	2	(Waclawiak and Kalisz 2012)	-
	d_{ref}	$17.53 \cdot 10^{-6}$	(Raclavská et al. 2017)	Average diameter of six smallest diameters from samples FA1 – FA3
TN98X18	E^*	$5 \cdot 10^{10}$	(Kleinhans et al. 2018)	Chosen from range of values in Table 29 (page 161)
	Γ	0.2	(Thornton and Ning 1998)	-
	ρ_y	$5 \cdot 10^8$	(Kleinhans et al. 2018)	Chosen from range of values in Table 20 (page 130)

Both models are reported separately as both groups of parameters do not necessarily describe identical properties of fly ash. For each set of nine simulations investigating the influence of parameter variation, factorial analysis was done for all individual size fractions using the Minitab 19 (Minitab, 2019).

3.1 WK12

The results of the factorial analysis show, that the d_{ref} (C) is significant for all six fractions. Constant in the Van der Waals force has significant effect only on smaller particles (6 μm and 19.5 μm), possibly showing low significance of the Van der Waals force on particle deposition.

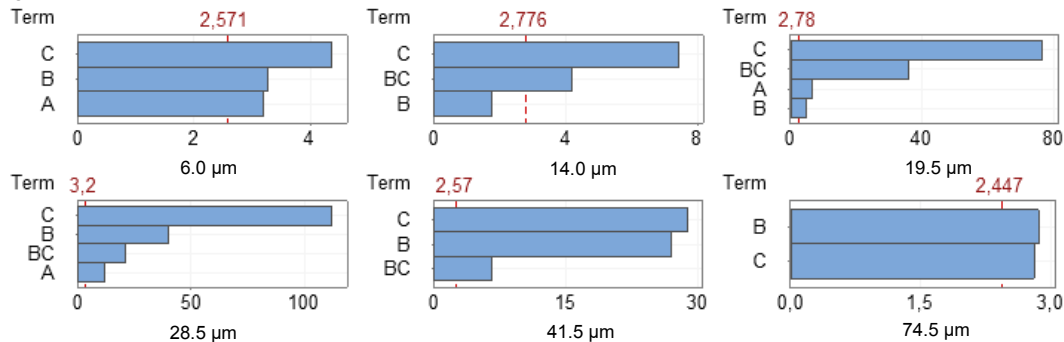


Figure 3: WK12 model. Standardized effects of significant terms of the model obtained by factorial analysis of data from simulations. Term (A) represents constant B , (B) exponent n and (C) reference diameter d_{ref} . (BC) represents interaction of factors (B) and (C).

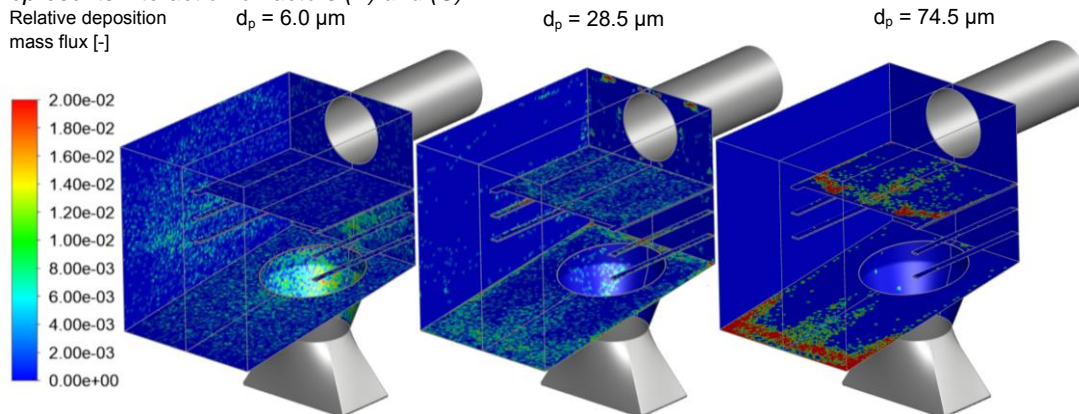


Figure 4: WK12 using reference values of parameters. Contours of deposition mass flux divided by the maximum flux value. Fluxes are reported separately for three size fractions.

3.2 TN98X18

The effect of the yield limit can be considered as the smallest for middle size fractions, while E^* and γ are significant for all investigated particle sizes. The only exception is the diameter $41.5 \mu\text{m}$, for which no parameter was identified as statistically significant. In contrast to WK12 model, only a modest deposition flux was observed on the chamber bottom and the baffle for the coarse fractions, at all tested combinations of parameters.

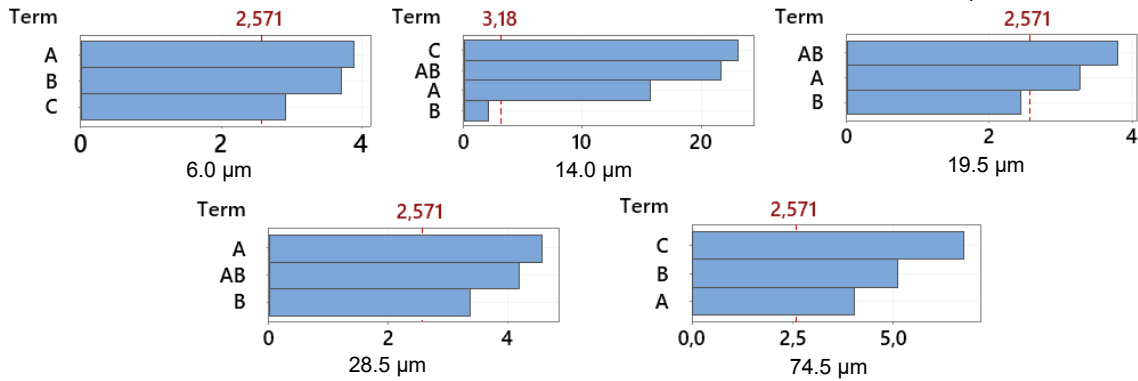


Figure 5: Standardized effects of significant terms of the model obtained by factorial analysis of data from simulations using TN98X18 model. (A) represents effective Young modulus E^* , (B) yield limit p_γ and (C) interface energy γ .

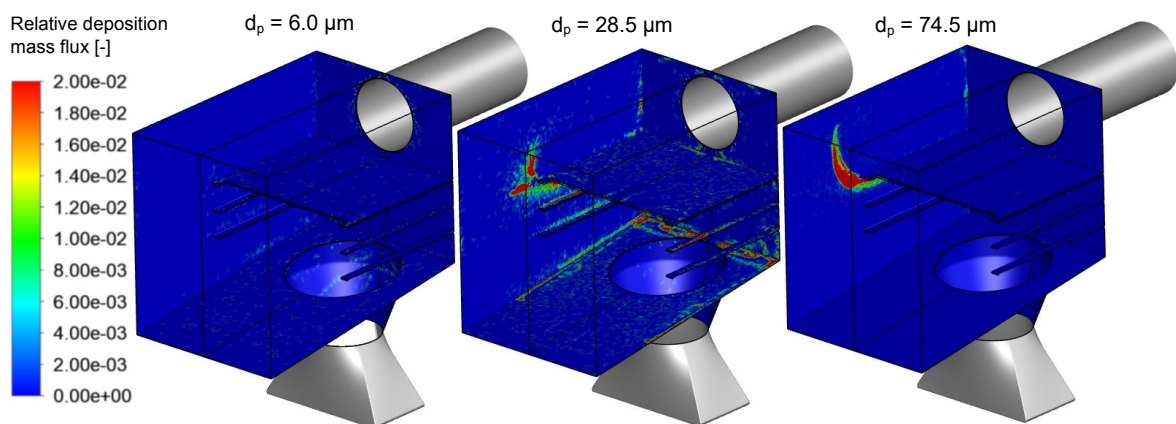


Figure 6: Model TN98X18 using reference values of parameters. Contours show deposition mass flux divided by the maximum flux value. Fluxes are reported separately for three size fractions.

4. Conclusions

WK12 – The results showed low sensitivity to value of the parameter B for larger particle diameters. Parameters n and d_{ref} express the elasticity of both the particle and surface and influence the particle regardless of its diameter. For the larger particles, the gravitational force is more prominent, which can be seen on the simulated deposition fluxes on the chamber bottom and upper side of the baffle. The d_{ref} was identified as the most significant parameter for middle values of particle diameters. Maximum variation of the predicted deposition mass flow rate was 38.8 % for the particle with diameter $14 \mu\text{m}$. Least affected were particles with diameter $28.5 \mu\text{m}$ and $41.5 \mu\text{m}$, where the difference between maximum and minimum deposition flow rate was 10.5 % and 11 %.

TN98X18 – Compared to the previous model, none of the parameters shown higher significance for any of particle fractions. For the diameters between $19.5 \mu\text{m}$ and $41.5 \mu\text{m}$, the interface energy was shown to be insignificant. Total deposition rate of particles with diameter $41.5 \mu\text{m}$ was reported to be insensitive to all three parameters.

From the obtained results it can be seen, that only for the first model, a general recommendation can be made. The reference diameter has the strongest influence for all tested particle diameters except for the largest particle diameter. When using the second model, the most important parameter depends on the particle diameter, implying the necessity of information about the size distribution.

Nomenclature

B – constant in WK12 model, $\text{kg}\cdot\text{m}^2/\text{s}^2$	n – exponent in WK12 model, -
d_p – particle diameter, m	v – velocity, m/s
d_{ref} – reference diameter WK12 model, m	v_s – sticking velocity, m/s
E^* – effective Young modulus, Pa	v_y – yield velocity, m/s
F_{el} – elastic rebound force, N	p_y – yield limit, Pa
F_g – gravitational force, N	α – angle, rad
F_{vW} – Van der Waals force, N	γ – interface energy, J/m ²
g – gravity acceleration, m/s ²	ρ – density, kg/m ³
G – constant in WK12 model, $\text{kg}/(\text{m}^2\cdot\text{s}^0.8)$	θ – angle, rad
m_p – particle mass, kg	ω – angular velocity, rad/s

Subscripts

i – impact	r – rebound
n – normal component	t – tangential component

Acknowledgements

The authors gratefully acknowledge the financial support provided by the Technology Agency of the Czech Republic (TACR) within the research project National centers of competence, specifically through the project National Centre for Energy (TN1000007).

References

- Ansys® Academic Research CFD, Ansys Fluent, Release 20.2.
- Cai Y., Kunlin T., Zhimin Z., Wenming Y., Hui W., Guang Z., Zhiwang L., Siah K.B., Subbaiah P., 2018, Modeling of Ash Formation and Deposition Processes in Coal and Biomass Fired Boilers: A Comprehensive Review, *Applied Energy*, 230, 1447–1544.
- Jegla Z., Kilkovský B., Stehlík P., 2010, Calculation Tool for Particulate Fouling Prevention of Tubular Heat Transfer Equipment, *Heat Transfer Engineering*, 31, 757–65.
- Kleinhans U., Wieland C., Frandsen F.J., Spliethoff H., 2018, Ash Formation and Deposition in Coal and Biomass Fired Combustion Systems: Progress and Challenges in the Field of Ash Particle Sticking and Rebound Behavior, *Progress in Energy and Combustion Science*, 68, 65–168.
- Minitab 19 Statistical Software, 2020.
- Raclavská H., Corsaro A., Hartmann-Koval S., Juchelková D., 2017, Enrichment and Distribution of 24 Elements within the Sub-Sieve Particle Size Distribution Ranges of Fly Ash from Wastes Incinerator Plants, *Journal of Environmental Management, Environmental management as a pillar for sustainable development*, 203, 1169–77.
- Stančin H., Mikulčić H., Wang X., Duić N., 2020, A Review on Alternative Fuels in Future Energy System, *Renewable and Sustainable Energy Reviews*, 128.
- Stehlík P., 2011, Conventional versus Specific Types of Heat Exchangers in the Case of Polluted Flue Gas as the Process Fluid – A Review, *Applied Thermal Engineering*, 31, 1–13.
- Strouhal J., Juřena T., Jegla T., 2020, Analysis of influence of model input parameters on ash fouling rate predicted by CFD, *Engineering Mechanics 2020*, 468–71.
- Thornton C., Ning Z., 1998, A Theoretical Model for the Stick/Bounce Behaviour of Adhesive, Elastic-Plastic Spheres, *Powder Technology*, 99, 154–62.
- Wacławiak K., Kalisz S., 2012, A Practical Numerical Approach for Prediction of Particulate Fouling in PC Boilers, *Fuel*, 97, 38–48.
- Weber R., Schaffel-Mancini N., Mancini M., Kupka T., 2013, Fly Ash Deposition Modelling: Requirements for Accurate Predictions of Particle Impaction on Tubes Using RANS-Based Computational Fluid Dynamics, *Fuel*, 108.
- Xie J., Dong M., Li S., Mei Y., Shang Y., 2018, An Experimental Study of Fly Ash Particle Oblique Impact with Stainless Surfaces, *Journal of Aerosol Science*, 123, 27–38.